

Article

Not peer-reviewed version

Ion-Specific Gelation and Internal Dynamics of Nanocellulose Biocompatible Hybrid Hydrogels: Insights from Fluctuation Analysis

Arianna Bartolomei , Elvira D'Amato , [Marina Scarpa](#) , [Greta Bergamaschi](#) , Alessandro Gori , [Paolo Bettotti](#) *

Posted Date: 14 February 2025

doi: 10.20944/preprints202502.1038.v1

Keywords: Nanocellulose; Hydrogels; Dynamic Light Scattering; Sol-gel transition; Cell Culture







Preprints.org is a free multidisciplinary platform providing preprint service that is dedicated to making early versions of research outputs permanently available and citable. Preprints posted at Preprints.org appear in Web of Science, Crossref, Google Scholar, Scilit, Europe PMC.

Copyright: This open access article is published under a Creative Commons CC BY 4.0 license, which permit the free download, distribution, and reuse, provided that the author and preprint are cited in any reuse.

Article

Ion-Specific Gelation and Internal Dynamics of Nanocellulose Biocompatible Hybrid Hydrogels: Insights from Fluctuation Analysis

Arianna Bartolomei ^{1,†}, Elvira D'Amato ¹, Marina Scarpa ¹ , Greta Bergamaschi ² ,
Alessandro Gori ²  and Paolo Bettotti ^{1,*} 

¹ Nanoscience Laboratory, Department of Physics, University of Trento, v. Sommarive 14, 38123 Povo, Trento, Italy.;
elvira.damato@unitn.it, marina.scarpa@unitn.it, paolo.bettotti@unitn.it

² National Research Council of Italy, Istituto di Chimica Del Riconoscimento Molecolare (ICRM), Via Mario Bianco, 9, Milano, 20131, Italy; greta.bergamaschi@cnr.it, alessandro.gori@cnr.it

* Correspondence: paolo.bettotti@unitn.it

[†] Current address: Department of Applied Physics, University of Granada.

Abstract: Hydrogels find widespread use in bioapplications for their ability to retain large amounts of water while maintaining structural integrity. In this article we investigate hybrid hydrogels made of nanocellulose and either amino-polyethyleneglycol or sodium alginates and we demonstrate two novel results: 1) the biocompatibility of the amino containing hybrid gel synthesized using a simplified receipt that does not require any intermediate synthetic step to functionalize either components and 2) the fact that the fluctuation of the 2nd order correlation function of a Dynamic Light Scattering experiment provides relevant information about the characteristic internal dynamic of the materials across the entire sol-gel transition as well as quantitative information about the ion-specific gel formation. This novel approach offers significantly better temporal (10's μ s) and spatial (10's μ m) resolution than many other state-of-the-art techniques commonly used for such analyses (such as rheometry, SAXS, and NMR) and it might find widespread application in the characterization of the nano to microscale dynamics in soft materials.

Keywords: nanocellulose; hydrogels; dynamic light scattering; sol-gel transition; cell culture

1. Introduction

Hydrogels are defined as three-dimensional networks capable of absorbing a large quantity of liquids. Given such broad definition, their composition and physico-chemical properties are highly tunable, as are their preparation and characterization methods[1]. So hydrogels are considered versatile materials with wide range of applications[2]. For instance, by using the appropriate components, smart functional hydrogels can respond to various external stimuli (such as pH, temperature, electric and mechanical stimuli) [3,4], or enable applications in advanced electronics [5], food industry [6] and biomedicine[7–9]. The expected increase in large scale applications requires to move toward sustainability and the use of natural polymers as hydrogel components offers an eco-friendly opportunity. In this regard, nanomaterials derived from cellulose sources are ideal candidates [10–13] with cellulose nanocrystals (CNC) showing a polymer-like behavior which quickly jellyfy upon addition of multivalent cations. The ionotropic gelation process is mediated by the interaction of the cations with the negatively charged or polar groups of CNC (mainly hydroxyls, carboxyls, carbonyls, sulfates, depending on the CNC's synthesis procedure) and allow precise control over the macroscopic gel structure [14–16] and the synthesis of hydrogels with controlled properties[17–21]. However, to overcome the intrinsic CNC stiffness and to obtain the desired mechanical properties, CNCs are often used as fillers of softer polymers [22–27]. The development of nanocellulose hybrid gels as substrates for cell cultures requires both an optimized synthesis process and a thorough characterization of their physical properties. In this study, we present a simplified synthesis approach that enhances the

reproducibility and scalability of the hybrid material while maintaining its structural integrity and biocompatibility. To further investigate the gel's physicochemical properties, we introduce a novel analysis of the correlation function obtained from dynamic light scattering (DLS) measurements. This refined analysis provides deeper insight into the gel network dynamics, shedding light on particle interactions and aggregation behavior. By linking the synthesis process with advanced characterization, we establish a more comprehensive understanding of how material properties influence cell culture performance, paving the way for improved biomaterials in tissue engineering and regenerative medicine applications. A simplified synthesis to fabricate an hybrid gel made of CNC and aminated PEG is an important result since this formulation strategically integrates materials with complementary chemical and mechanical properties and it enables the creation of versatile hydrogel platforms. In fact, while cellulose contributes with carboxyl groups, amino-PEG introduces valuable amine functionalities to the matrix, establishing a dual-functionality system. The presence of both amine and carboxyl groups is particularly advantageous for bio-applications, as these functional groups can facilitate cell adhesion, protein binding, and potential crosslinking through various chemical reactions such as amide bond formation. Amines functionalities can be directly added to CNC[28,29] but the reaction is time-consuming and care should be taken to avoid unexpected gelation and the cross-linking of amine and carboxylic groups. Thus, this strategy is mainly limited to dilute nanocellulosic solutions. Several studies report on the use of amino-PEG and CNC to form hybrid gels but they mostly use diacrylate-PEG and they require a dedicated step to cross-polymerize PEG and CNC. For example in [30,31], the authors report the synthesis of a photopolymerizable 3D PEG diacrylate (PEGDA) ink in which CNC is used as a filler to increase the mechanical properties. Similarly, [32,33] report the use of PEGDA-CNC composites to form gels with variable Poisson ratios. In [34], a 3D printable bioink is formed by mixing a nanocellulosic solution with a 4-arms star PEG polymer and by photopolymerizing the resulting viscous fluid. Ref. [35] demonstrates the synthesis of an hybrid hydrogel by crosslinking PEG and CNC with acrylamide and N,N'-methylene bis-acrylamide. In [36], 8-arm branched amino PEG polymer is acrylated and photopolymerized under UV irradiation. [37] is the only report that demonstrated the possibility to obtain hydrogels by direct mixing micron-sized cellulosic fibers with branched, tetra-arms amino-PEG. Our approach takes a step forward compared to what has been shown so far and demonstrates the possibility to synthesize biocompatible hybrid gels by simply mixing CNCs and linear amino-PEG. Moreover, although the biocompatibility of hybrid gels made of CNCs and PEG have been demonstrated [38–40], similar results are unreported for amino-PEG and CNC hybrid gels.

From the perspective of characterization methods, we have developed an innovative approach to analyze DLS measurements that exploits the statistical properties of the 2nd order correlation function measured from a commercial, DLS instruments at single scattering angle to correlate information about the sol-gel transition and the material composition. To demonstrate this possibility we exploit the peculiar characteristic of alginates to jelly in the presence of Ca^{2+} but not with Mg^{2+} [41,42] and we show that the statistical properties of the measured 2nd order correlation function contains information about the sol-gel transition dynamics and also about the material composition. We define a phenomenological Figure of Merit (FOM), based on the short-time values of the 2nd order correlation function, and the comparison among the two families of materials (i.e. the Ca^{2+} crosslinked gel and the Mg^{2+} suspension) unveil the differences in their internal dynamics.

The cation complexes of alginates have an intriguing nature and their role in the hydrogel network formation is currently matter of research [43].

Different methods spanning from the atomic scale up to the microscale are necessary to characterize the structural morphology, composition, and mechanical properties of hydrogels. The advantages and disadvantages of these methods have been recently reviewed concluding that the hydrogel characterization remains challenging also because of the hierarchical length scales of the network structure [44]. In general, the most popular approach to investigate the macroscopic mechanical properties is the rheological analysis. This method allows for the investigation of sol-gel transition and provides

quantitative information about the macroscopic properties of the material [45]. Yet, routine rheology experiments cannot sense the fine details of the gel structures and different materials can share similar macroscopic mechanical properties (like the elastic, and viscous modulus) while differing in their local structure. Advanced rheological techniques such as dynamic shear rheology and large amplitude oscillatory shear experiments are very promising investigative tools of the dynamics of gelation of thixotropic suspensions. However, the complexity of data analysis and the necessity of integrative structural information restrict their use to few material and require skilled researchers [46].

Dynamic Light Scattering (DLS) that is a family of techniques that exploit scattering of light to investigate structural and dynamical details of colloidal particles and gel dynamics. Despite their basic theory has been thoroughly developed starting from 1950's [47–50], the complex interpretation of the data and the strong assumptions on which models are based make DLS a lively research field even today with several variants proposed in recent years to overcome some of the limits of the techniques [51–53]. One of the weak points of experimental data interpretation of any DLS technique is the assumption about the type of motion of the particles and/or their size distribution. In fact, these methods require a transformation from the experimentally measured quantity (the light intensity that produces the 2nd order correlation function) to the 1st order correlation function that relates how the electromagnetic field interacts and is scattered by the illuminated sample structure. Standard DLS measure cannot handle highly turbid samples (as often gels are), since they assume single scattering event and are thus compatible only with dilute solutions. Moreover systems undergoing irreversible dynamics (non ergodic) require specialized setups where scattering is averaged by moving the sample and investigating different positions. On the other hand, diffuse wave spectroscopy provides information about highly scattering samples, but in this case, a large number of scattering events is required to properly describe the light scattering as a diffusive process [54–56]. The intermediate range, that is the dynamic one formed *during* the sol-gel transition, is poorly investigated since there are no analytical models able to handle the complexity of the transient between the sol and the gel regimes. In order to fill this gap and investigate the dynamics at the nanoscale of a solgel transition we used the statistical properties of the light scattered during a DLS experiment and proved that they contain relevant information about the dynamics of the sol-gel transition and from its analysis we can distinguish samples that differ in the relative amounts of their components.

2. Materials and Methods

2.1. Materials

Commercial wood pulp Celeste 85 has been kindly provided by SCA (Sweden). TEMPO 2,2,6,6-tetramethylpiperidine-1-oxyl (TEMPO) 98+% purchased by Alfa Aesar; NaBr 99% and NaOH 1 M produced by Carlo Erba and NaClO solution with 6-14% active chlorine produced by EMPLURA were used. Bis(3-aminopropyl) terminated PEG, with average molecular weight of ~ 1500 Da, purchased by Sigma-Aldrich and alginic acid sodium salt solution with very low viscosity, purchased by Thermo Fisher Scientific Chemicals were used to realize CNC hybrid hydrogels. All chemicals have been used as received, without further purification. MilliQ grade water has been used for all preparations and processes. HeLa cells were cultivated in DMEM containing phenol red and supplemented with 10% Fetal Bovine Serum (FBS), 2 mM glutamine, 100 U/ml penicillin and 100 µg/ml Streptomycin (Pen-Strep). PBS (pH 7.4), Trypsin-EDTA 0.25% and phenol red were used to wash cells before dissociation and for trypsinization, respectively. Trypan Blue Solution, 0.4% was used to stain alive cells to be counted in a Burker chamber hemocytometer. For MTT assays, phenol red-free DMEM supplemented with FBS, Pen-Strep and L-Glutamine was used since it is proven that phenol red compromises the outcome of MTT assays. CyQuant MTT kit, was used to assess cell viability. All the listed chemicals were purchased by Gibco-Thermo Fisher Scientific.

2.2. Synthesis of CNC

TEMPO-oxidized CNC has been produced with a slightly modified receipt from[57]. Briefly: 10 g of cellulose pulp are swollen in 500 ml of distilled water for 5 hours at room temperature under stirring and then sonicated in bath for 30 min. 160 mg of TEMPO and 1 g of NaBr salt are added and the final volume is brought to 1 l. The oxidation is started by addition of 35 ml of NaClO and left to proceed for 3 hours keeping the pH at 10.5 by addition of 1 M NaOH. The slurry is rinsed 5 times by plenty of distilled water and divided in 35 ml aliquots. Each aliquot is sonicated with a Bandelin Sonopuls HD 2200 ultrasonic homogeneizer equipped with a 13 mm tip, settled at 160W and then vacuum filtered over a 5 μ m cellulose acetate filter (Sartorius, Germany). The CNC suspension is heated at 70 °C in a water bath under magnetic stirring until a concentration of 7 mg/mL is obtained. Finally, the suspension is again vacuum filtered to remove residual impurities.

2.3. Synthesis of Hybrid Gels

CNC-PEG hybrids (NP) were prepared in the following way: 200 mg of bis(3-aminopropyl) terminated PEG were dissolved in 10 ml of deionized water and stirred until a homogeneous solution was achieved. Subsequently, HCl (1 M) was added until the pH reaches $7.2 \div 7.4$. The resulting suspension was then filtered using a 0.22 μ m pore-size filter with a PES membrane. Following filtration, it was mixed with a 7 mg/ml CNC solution in two different volume ratios: CNC:PEG = 2:1 and CNC:PEG = 3:1. CNC-alginate hybrids (NA) were similarly prepared: 2.5 g of alginic acid sodium salt were dissolved in 100 ml of DI water, to get a 2.5% w/v aqueous solution. It was then filtered with a 0.45 μ m pore-size filter with PES membrane and later mixed with the CNC solution in two different volume ratios: CNC:Alginate = 2:1 and CNC:Alginate = 3:1. The several compositions of the hydrogels under study are summarized in Table 1. Hybrid hydrogels were crosslinked by dropping a 1 M $MgCl_2$ solution with a pipette along the inner border of polystyrene cuvettes/multiwells already containing the CNC-based solution, such that the final Mg^{2+} concentration is 47.6 mM (we will round it up to 50 mM for the rest of the paper).

Table 1. Details of the composition of hydrogels. Numbers indicates the relative volumes of the constituents.

Name	CNC	PEG	Alginate
CNC	1	0	0
NP2	2	1	0
NP3	3	1	0
NA2	2	0	1
NA3	3	0	1

When used for cell culture experiments, all CNC-based solutions (pure CNC and hybrids) were sterilized in an autoclave at 1 bar and 121 °C for 1 h.

2.4. Hydrogels Characterization

CNC was structurally characterized via Atomic Force Microscopy. NT-MDT SMENA head equipped with NSG-10 tip (elastic const.: 11.8 N/m and typical resonant freq.: 240 kHz) was used to measure the average CNC dimensions.

Fourier Transform Infrared spectra of both pure CNC and hybrid materials were acquired with a Nicolet FTIR microscope at standard spectral resolution (4 cm^{-1}) and a suitable number of acquisitions (typically 64) for a good signal-to-noise value.

Rheological properties of hydrogels were evaluated with a Malvern Panalytic KINEXUS PRO+ rheometer equipped with a plate-plate geometry (diameter: 20 mm). The upper geometry plate was lowered until it was in conformal contact with the top surface of the hydrogel, corresponding to gap distance of 1mm. Samples were preformed, directly transfer on the bottom plate, and equilibrated for 5-minute resting time in the instrument. Dynamic moduli and elastic response under oscillatory

stresses were assessed through strain sweep experiments to estimate the LVER (frequency = 1 Hz, strain 0.01% to 10%) and frequency sweep (frequency ranging from 0.1 Hz to 100 Hz, constant stress chosen within the LVER). The shear rate dependence of viscosity was studied within a shear ramp $\dot{\gamma} = 1\text{--}100\text{ s}^{-1}$. All measurements were repeated at least three times and carried out at a constant temperature of 25 °C. Dynamic Light Scattering (DLS) characterization was carried out with an Anton-Paar Litesizer 500 DLS machine, used in the 90° angle configuration. In this case, 100 μl of 1 M MgCl_2 aqueous solution is added directly into the DLS cuvette that contains 2 ml of any of the CNC suspension. The DLS measure starts soon after the addition of the cations and last for hours.

2.5. Cell Culture and Cell Viability

HeLa cells were used, since this cell line is considered a versatile model to test the biocompatibility of the substrates[58]. The cells were directly seeded on the material under study and the survival and growth rate were quantified by colorimetric, fluorimetric and cytometric assays.

To assess cell survival on the hydrogels, two 48-wells plates were used to culture HeLa cells, extracted from the same cell line, to perform MTT assays after 48 and 96 hours of incubation. Triplicates of the five CNC-based hydrogels under study were prepared in each multiwell plate by adding 20 μl of a sterile 1 M MgCl_2 aqueous solution to each well containing 400 μl of CNC-based solution, for each composition. Prior to use, the five CNC-based suspensions were autoclaved, while the MgCl_2 aqueous solution was filtered with a 0.22 μm pore size filter. The multiwell plates containing the hydrogels were left unperturbed overnight to complete gelation and then they were rinsed 5 times with sterile DI water before adding 2 ml of pure phenol-red DMEM to each well. In this way, DMEM could diffuse inside the hydrogels and exchange with water under the effect of the concentration gradient. After at least 3 hours of incubation at 37 °C and in a 5% v/v CO_2 atmosphere, the excess supernatant above each hydrogel was removed and substituted with 2 ml of freshly supplemented phenol red-free DMEM to increase the amount of nutrients stored inside the gel. After a second incubation of at least 3 hours, another exchange with supplemented phenol red-free DMEM was done, such that the concentrations of FBS, Pen-Strep and L-Glutamine inside the gels could increase up to the standard ones. HeLa cells were seeded on the hydrogels with an areal cell density of 10^3 cells/ml, which was spotted to be the optimal one during a preliminary trial. The same areal cell density was seeded in triplicate on pure polystyrene as reference. MTT assay were performed at two different incubation times (48 h and 96 h) to verify cells interaction with the substrates and their growth rate. After incubation, the MTT protocol was followed to quantify the metabolic activity of HeLa cells: 1 ml of sterile PBS, thermalized at 37 °C, was added to one vial containing 5 mg of MTT, to prepare the 12 mM MTT solution to drop in each well with a cell culture. Indeed, after having substituted the old culture medium with 300 μl of fresh supplemented DMEM without phenol red in each well, 30 μl of the MTT solution were added to each well to test. After 4 hours of incubation, 300 μl of 0.1 mg/ml SDS solution at pH 2 were added to the culture medium to dissolve the formazan crystals formed by alive cells. After 15 hours of incubation, absorbance at 570 nm of the culture medium in each well was read with an Infinite M200 PRO microplate reader by Tecan. For the reading, the area of each well was sampled 25 times.

2.6. DLS Analysis

According to the objective of our research, we investigated the possibility of using DLS data to unravel the nanoscale dynamics of the 3D hydrogel network formation during an ionotropic gelation process. Below a brief survey of the relevant equations is reported to clarify the idea behind the DLS data analysis performed, while more detailed descriptions can be found in dedicated literature cited above.

In DLS an electromagnetic field is used to track the dynamics of scatterers. If there is a relative movement between the scatterers and the illuminated volume, then the scattered light fluctuates in time. The detector of the DLS tracks these fluctuations and constructs the so called time-average normalized intensity correlation function: $g^{(2)}(k, \tau) = \frac{\langle I(k,0)I(k,\tau) \rangle_T}{\langle I(k,0) \rangle^2}$, where $k = \frac{4\pi n}{\lambda} \sin(\theta/2)$ is the

k -vector of the scattered light, n is the solvent refractive index, λ is the laser wavelength (elastic scattering is assumed) and θ is the angle at which light is collected with respect to the incident laser direction. $\langle \dots \rangle_T$ indicates a time average, that is: each measurement (run) is divided in N temporal bins and the numerator of $g^{(2)}(\tau)$ is $\frac{1}{N} \sum_{i=1}^N \chi(i \cdot T) \cdot \chi(i \cdot T + \tau)$, where χ is the number of photons collected within the iT -th bin (the normalization value at the denominator is of no relevance for our purposes). This analysis is performed by a dedicated electronic (the correlator) [47].

In the case of dilute colloidal solution, where scatterers freely diffuse with Brownian dynamics, long enough measures allow to average over all possible configurations of the colloids, that is $g^{(2)}(\tau)$ contains all the information to fully describe the average system dynamics. On the contrary, in systems where scatterers are not free to move (eg. within a gel), the temporal averaged $g^{(2)}(\tau)$ does not sample all the possible structural configurations of the scatterers and it provides a biased estimation (ie. incomplete) of the system dynamics. These systems are said non-ergodic and a proper sampling of their properties requires an ensemble averaging that is a time average replicated in several different spatial positions, to be sure to collect the dynamics from most of the possible structural configurations and, thus, to get a reasonable estimate of the system dynamics.

The statistical behavior of $g^{(2)}(\tau \rightarrow 0)$ changes depending if the system is (non)-ergodic. In particular[48]:

- $g^{(2)}(\tau \rightarrow 0) = 2$ in solutions (ergodic systems)
- $1 < g^{(2)}(\tau \rightarrow 0) < 2$ in gels
- $g^{(2)}(\tau) \sim 1$ in glasses (completely freezed systems)

Generally DLS retrieves information about the particle size by assuming dilute and ergodic samples. In this case the field scattering time-correlation function is given by the Siegert relation: $g^{(2)}(\tau) = |g^{(1)}(\tau)|^2 + 1$, where $g^{(1)}(\tau)$ is the Laplace transform of the characteristic decay rates: $g^{(1)}(\tau) = \int_0^\infty G(\Gamma) \cdot \exp(-\Gamma\tau) d\Gamma$, where D is the characteristic decay time (ie. the time the colloid takes to flow across the illuminated volume and it depends on both the solvent viscosity and the colloid size). In the case of monodispersed samples there is just a single D and $g^{(1)}(k, \tau) = \exp(-Dk^2\tau)$. By exploiting the Stokes-Einstein equation, the hydrodynamic radius of the colloid is extracted: $R_H = \frac{k_B T}{6\pi\eta D}$.

The gel building blocks are not free to diffuse. A basic model describes the gel scatterers as fluctuating around an average stable position. The overall light scattering is the superposition of two contributions:

- one coming from the "freezed", averaged configurations of the scatterers,
- one due to the fluctuations around their average position.

Despite this apparently simple decomposition of the motion, the formulation of a model able to quantitatively describe the gel case is a formidable task, yet to be solved and it requires a detailed knowledge of the actual system under study (both physical and chemical details).

Actual DLS correlators, routinely record delays down to 100's ns. These timescales are much faster than the typical transit time of a colloidal particle over the volume illuminated by the laser. In fact, consider a spherical colloid of about 100 nm size, freely diffusing in water at 298 K. From the Stokes-Einstein equation, $D \sim 10^{-12} \text{ m}^2/\text{s}$. For a Brownian motion in 1D systems, the average displacement is: $\langle x^2 \rangle = 2Dt$. Considering a 20 μm diameter illuminated volume, the time the colloid takes to cross it is: $t = \frac{\langle x^2 \rangle}{2D} \sim 10\text{s}$. This demonstrates the idea that the first points of the $g^{(2)}(\tau \rightarrow 0)$ contains information about the fast gel dynamics and can be used to monitor its structural evolution as well as its internal dynamics. To ease the notation, in the rest of the paper we define $\sigma^2 = g^{(2)}(k, \tau \rightarrow 0)$, since this is the relevant value to define our FOM. It should be remarked that the information provided by our approach is complementary and not-overlapping to those provided by rheology. In fact while DLS investigates the microscopic system dynamic evolution, rheology monitors the macroscopic gel slow timescale evolution, even at the sol-gel transition point.

DLS measurements were performed as follows: each gel composition has been measured in triplicate and for each measurement we recorded several hundreds of autocorrelation runs, each of

5 s of duration. The exact number of runs depends on the sample since the induction time before σ^2 decreases cannot be controlled (it depends on how $MgCl_2$ diffuses in the cuvette).

The FOM is defined as the frequency of the fluctuations of σ^2 and it is calculated as follows: we average the first 20 points of each runs to calculate the value of the σ^2 (these points correspond to the time interval between 200 ns and 1 μ s). Then, we define a threshold value (see below) for the σ^2 function (called T) and we locate the time when σ^2 decreases below this threshold (at time $t = t_0$). To normalize the frequency vs the duration of the experiment, we calculate the frequency at which σ^2 crosses T as the number of crossing (c) divided by the duration of the measurement $t_T < t < t_f$: $FOM = c / (t_f - t_T)$, with t_T is the time corresponding to the threshold and t_f the total duration of the experiment. The optimal threshold has been selected using a dynamic programming algorithm [59]: it aims at minimizing a cost function with respect to the optimal partitioning of the dataset:

$$V(\mathcal{T}, y) := \sum_{k=0}^K c(y_{t_k}^{t_{k+1}}) \quad (1)$$

where V is the quantitative criterion function to be optimized (minimized in our case), $\mathcal{T} = \{t_1, t_2, \dots, t_k\}$ is the set of indexes that partition the signal y . Thus, V is given by the sum of the cost functions (denoted by c) for each signal partition $y_{t_k}^{t_{k+1}}$. Since we know the number of thresholds in our data (a single threshold), the optimal solution is computed by:

$$\min_{|\mathcal{T}|=K} V(\mathcal{T}, y) = \min_{0=t_0 < t_1 < \dots < t_K < t_{K+1}=T} \sum_{k=0}^K c(y_{t_k}^{t_{k+1}}) \quad (2)$$

3. Results and Discussion

CNC was structurally characterized with AFM and a representative image of CNCs is reported in Figure 1(a). The results of the statistical analysis of CNC sizes is shown in Figure 1(b). Nanocrystals have an average length of about 170 nm, broadly distributed with a St.Dev. of about 120 nm, while their height lies between 2 and 5 nm (averaged over more than 300 CNCs). DLS analysis confirms this data as reported in Figure 1(c). The structure is compatible with the usual one obtained from the TEMPO-mediated oxidation synthetic pathway.

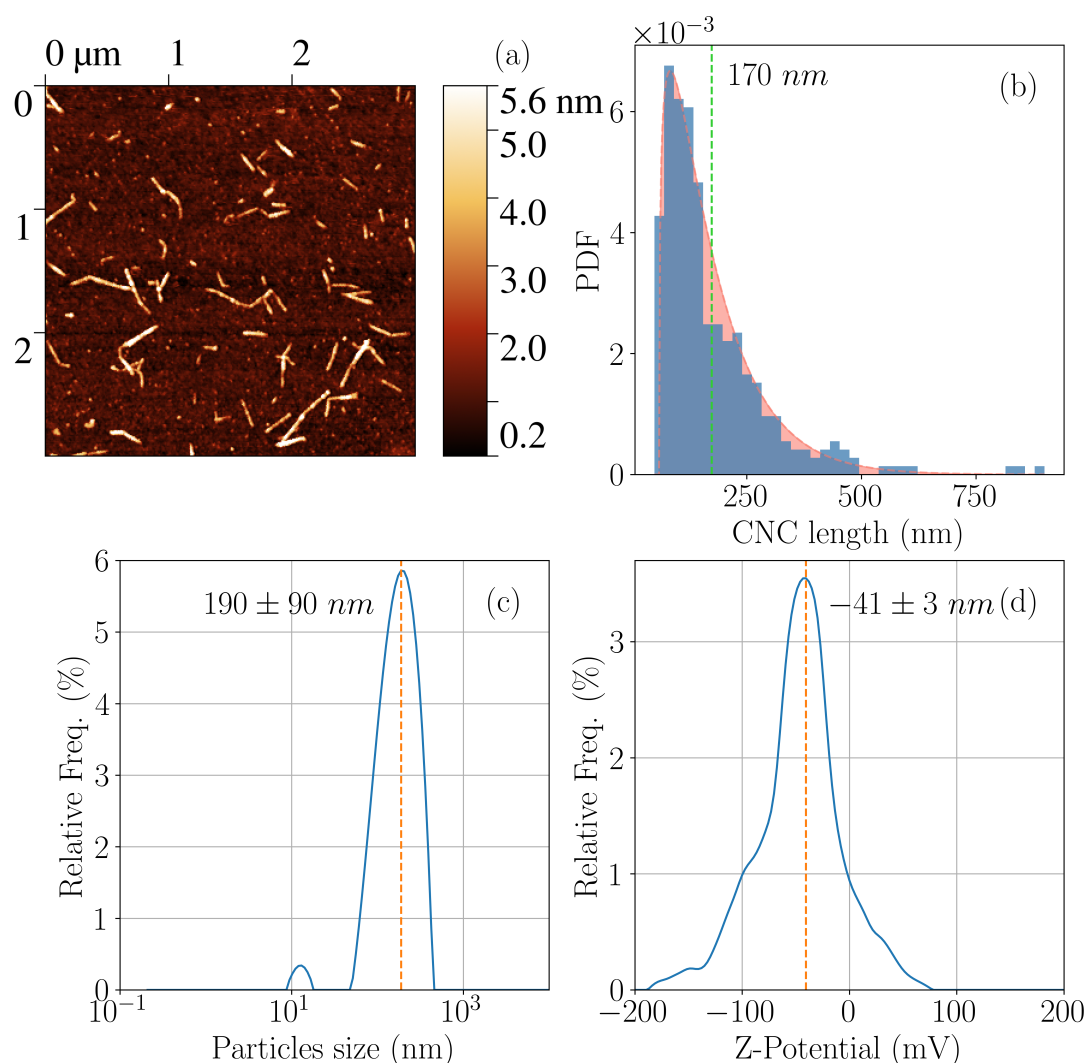


Figure 1. (a) Tapping mode AFM image of representative CNCs. (b) Histogram of the probability distribution function of CNC size, the green dotted line indicates the average CNC length. (c) The DLS analysis of a similar CNC sample confirms the average size of the nanocrystals. (d) The Z-potential analysis shows the negative surface potential of CNCs due to the presence of hydroxyls as well as carboxylic groups.

The presence of carboxylic groups on the surface of CNC is confirmed by FTIR spectroscopy and reported in Figure 2: the spectrum of pure and hybrid CNC gels (NA3 and NP3, see Table 1 for the sample composition) have been vertically shifted and rescaled to make relevant spectral signatures overlap. No baseline corrections have been applied. The significant spectral region is below 1800 cm^{-1} . Looking at CNC spectrum, the strong peak at 1600 cm^{-1} marks the COO^- asymmetric stretching, while the one at 1420 cm^{-1} refers to the symmetric one. The $\text{C}-\text{O}-\text{C}$ stretching is underlined by the peak at 1160 cm^{-1} [60,61]. The triplet between 1030 and 1110 cm^{-1} confirms the high crystallinity degree of the CNC [61]. A more detailed assignment of FTIR peaks can be found in the ESI.

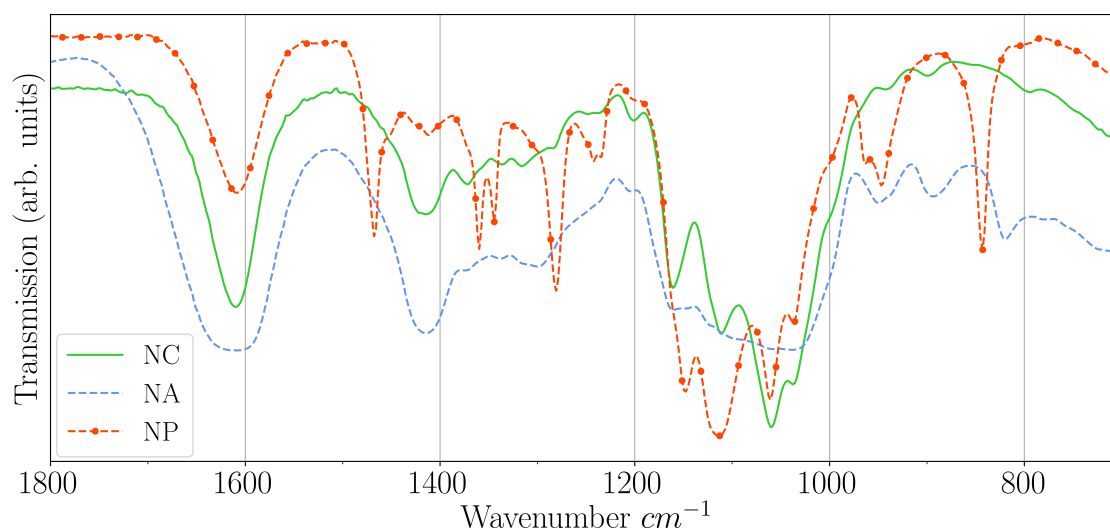


Figure 2. FTIR spectra of CNC (green continuous line), CNC-alginate (blue dotted line) and CNC-PEG (red dot-dash line) hybrids. While the materials that create an extended network of intermolecular bonds (CNC and NA) show broad absorption peaks, the NP samples keep the detailed vibrational structure of the PEG alone, thus supporting the fact of the small affinity between Mg^{2+} cations and the polymer.

The spectra of hybrid materials maintain the typical feature of pure polymers, suggesting that the interactions that form the gel do not significantly modify the vibrational degrees of freedom of the polymer chains. Consequently, the main role in forming the gel seems to be due to the CNC, while CNC-polymers interaction is of less importance. This hypothesis is supported also by the evidence that the stiffer gels are those formed by pure CNC (see Figure 3(a)).

Finally, the zeta potential of TEMPO-oxidized CNC is shown in Figure 1(d) and clearly shows a large negative value of the surface potential, compatible with those typically reported in literature and mainly ascribed to the presence of deprotonated carboxylic groups. Rheological analysis characterized the elastic and viscous moduli (G' and G'') of the gels and the results within the LVER are reported in Figure 3(a). Generally, both moduli increase in the order $CNC > NP > NA$ and for both CNC and NA the elastic modulus increases proportionally with the concentration of CNC. This fact is compatible with an overall stiffening of the gel framework, despite the poor affinity of Mg^{2+} with alginates in the case of NA hybrids. On the other hand, for a given ratio CNC/PEG, NP samples show a nearly constant G' up to an $MgCl_2$ concentration of 30 mM and only above this value their G' increases with a slope similar to that of the other compositions. Moreover, NP samples have slightly larger G moduli for low ionic strength compared with alginate hybrids. These considerations are confirmed by the viscosity characterization reported in Figure 3(b). All hybrids show the shear thinning behaviour typical of CNC suspensions [62], with a marked reduction of their viscosity over a range of about two orders of magnitudes at large shear frequencies. Pure CNC is the most viscous sample since the electrostatic interaction among CNCs is the strongest and the mesh size in the gel network is the smallest. All other samples show similar viscosities.

It should be noted that, despite the literature reports a variation of the elastic modulus over more than an order of magnitude (from 10^3 to 10^4 Pa [14,63]), the effectively exploitable range is limited by the equilibrium condition established within the gel during its actual use. Indeed, as already pointed out[15], the concentration of the crosslinking cation reaches a steady state value, independently of the amount of cations used during the gelation step. Moreover, increasing the mechanical properties of the gel by using a large excess of cations might produce unwanted results (e.g. toxic gels which release excess ions when used).

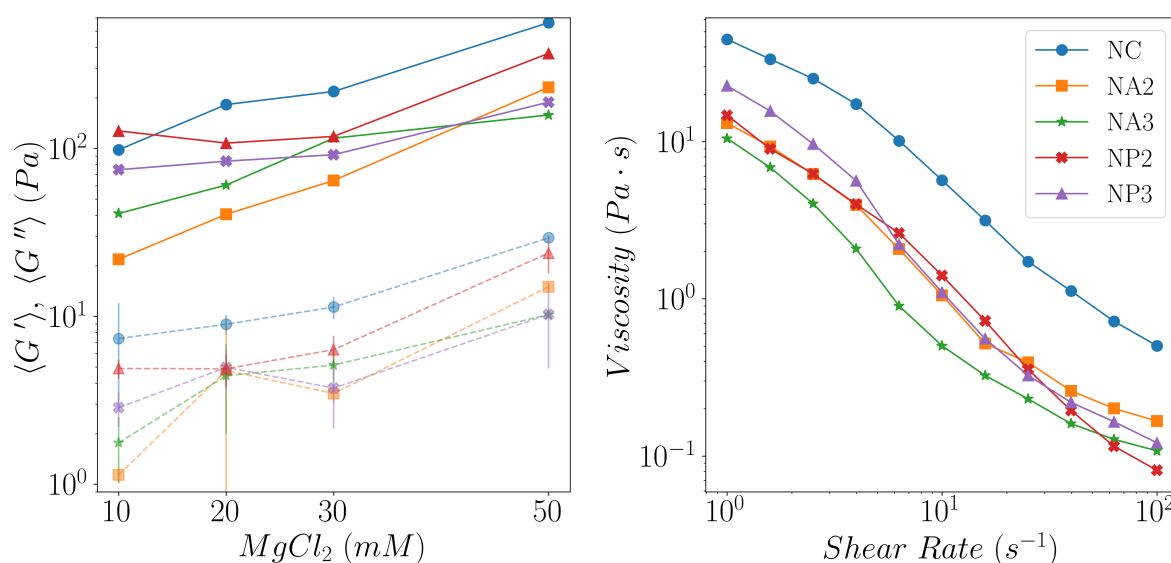


Figure 3. (left) G' and G'' values obtained from strain sweep experiments (see Figures 2 and 3 ESI) at increased concentration of $MgCl_2$ for all the tested CNCs. (Right) Viscometry shear rate ramp.

For applications such as cell cultures and, in particular, in the field of tissue engineering, where cells are embedded into an artificial ECM, it is of paramount importance to understand the actual state of the material internal architecture. DLS can provide information about the dynamics of the gels during their ageing and show how materials with similar macroscopic mechanical behaviour might have very different microstructures and dynamics, which can impact on their biocompatibility.

Figure 4 reports the dynamic of $\langle \sigma^2 \rangle$ for representative samples for each investigated composition (data for all samples can be found in the ESI). Initially, the systems are in a colloidal suspension state of barely interacting species and the $\langle \sigma^2 \rangle$ tends to the ideal value of 2, typical of ergodic systems. Upon the addition of $MgCl_2$, cations crosslink the species into clusters of increasing size and the suspension immediately jellifies, creating a solidified blob within the cuvette. Since the $MgCl_2$ solution is added at once within the DLS cuvette the dynamics of cation diffusion is stochastic in nature and the induction time before $\langle \sigma^2 \rangle$ decreases cannot be estimated in advance. Yet, all samples show a sharp drop of $\langle \sigma^2 \rangle$ by roughly an order of magnitude after a variable induction time. The optimal threshold for each sample is indicated by the different background color of Figure 4 panels. This phenomenon is the signature of a strongly reduced mobility of the particles (regardless if they are CNCs or polymer molecules), which is induced by the large concentration gradient of cations that quickly rearrange the structure of the system, from a solution into a gel network. The fast dynamics within the scattering volume destroys the coherence required to form significant autocorrelation, thus $\langle \sigma^2 \rangle$ collapses. Moreover the $\langle \sigma^2 \rangle$ fluctuations testify that the initially formed gel network is a metastable structure slowly evolving towards its equilibrium configuration. In the end, by tracking $\langle \sigma^2 \rangle$ it is possible to have a hint on the dynamic of the sol-gel transition of the system.

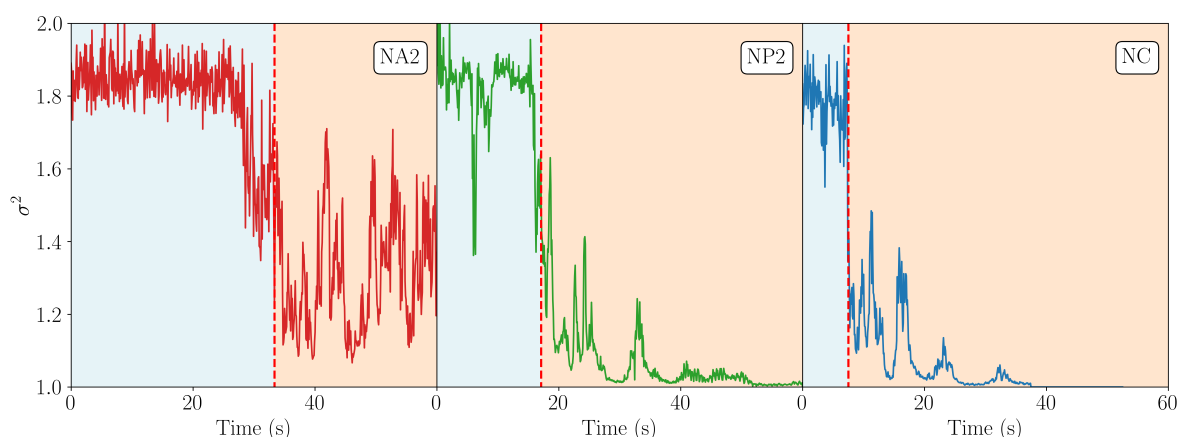


Figure 4. σ^2 dynamics versus time for representative sample of each composition (indicated by the legend). The different background colors indicate the optimal threshold. Data for each samples investigated are reported in the ESI.

The FOM for the five different compositions, for the optimal T -value, is reported in Figure 5.

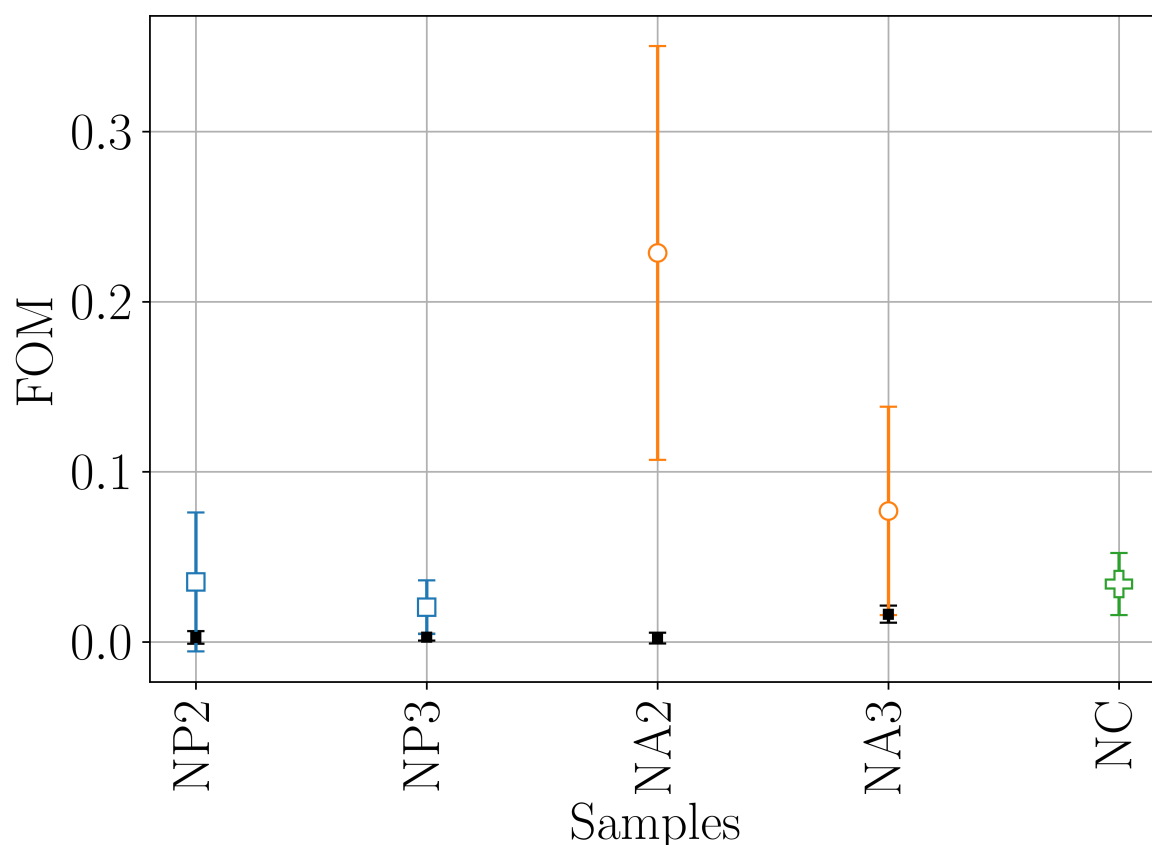


Figure 5. Classification of the different samples based on the FOM (using an $L1$ norm cost function). Coloured dots refer to the gelation using Mg as crosslinker, small black dots are for same hybrid compositions but jellified using Ca^{2+} .

CNC and NP samples share similar dynamics, with σ^2 decreasing sharply and mostly assuming small values after the transition occurs. On the other hand, NA samples show a marked decrease of σ^2 from its initial value but then it continues to oscillate for the entire time window considered. Pure CNC samples are reported for illustrative purposes and their FOM is comparable to those of the NP samples, suggesting a similar gelation dynamics for CNCs and NPs. NAs have a marked different behaviour and, by increasing the amount of CNC in the hybrids, the FOM decreases, tending to the one

of pure CNC. This fact supports the idea that our phenomenological parameter effectively represents a physical feature of the internal dynamics of the gel.

The dynamics of σ^2 can be understood by the following reasoning: upon addition of the crosslinker, $MgCl_2$, a non-equilibrium jellifying blob forms nearly instantaneously. Then, strong diffusive fluxes establish from the blob to equilibrate its composition. These diffusive processes destroy the coherence required to measure the typical (flipped) sigmoidal profile of $g^2(t)$. Moreover, since these fluxes affect the entire volume of the cuvette, multiscattering events take place along the optical path of the laser, thus, further decreasing the characteristic decay time and σ^2 . The difference between CNCs/NPs and NAs is due to their different aptitude to jellify: while CNCs and NPs form "stable" structures upon coordination with Mg^{2+} cations, the NAs maintain their internal dynamics. Alginate chains act as a viscous liquid reservoir that traps jellified particles of CNC and these latter are responsible for the fluctuations in σ^2 function. Again, given the large concentration and the broad dispersion in size of these CNC particles, no quantitative analysis can be performed on the $g^2(\tau)$ runs.

To verify the reliability of our approach we repeat the analysis for the same samples composition but using Ca^{2+} : in these cases the cation binds both PEG and alginates and the σ^2 always produced a small FOM, comparable to that of the pure CNC. This result confirms the strong affinity of Ca^{2+} with both cellulose and polymers and its role as effective crosslinker.

Finally, the hybrids were used as substrates for cell cultures. HeLa cells were used as model cell lines and were seeded with an initial areal cell density of $3.5 \cdot 10^3 \frac{cells}{cm^2}$.

Cell cultures were incubated up to 96 h. Cell viability was verified using standard MTT assay. The results are reported in Figure 6.

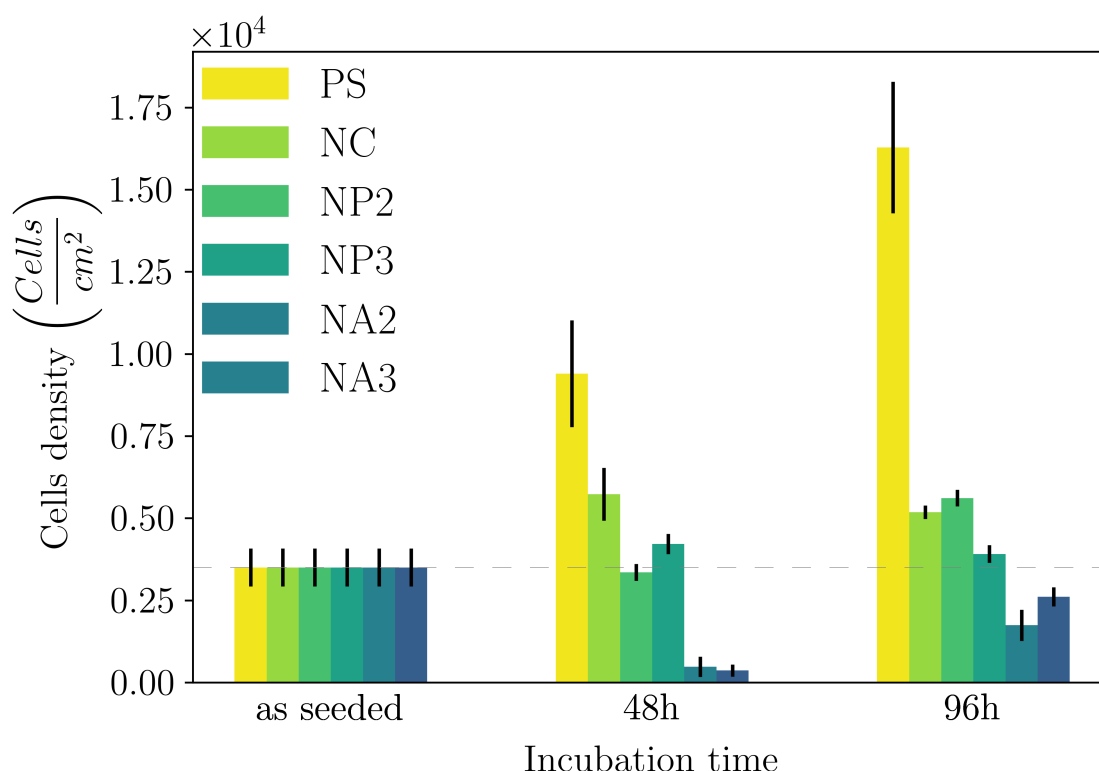


Figure 6. Results of MTT assay: metabolic cell viability expressed as areal cell density vs. incubation time for reference polystyrene and hydrogels. The dotted horizontal line is a guide for the eye, corresponding to the seeded areal cell density.

HeLa cells adhered within 24 hours and exhibited growth over time on any of the five CNC-based hydrogels, with varying growth rates. Compared to the reference polystyrene dishes, all gels show a

slowed cell growth, yet both CNCs and NPs show a constant increase of the cell number, while NAs hybrids initially hinder cell viability, albeit they also show an increase in cell number with time.

It is well known that, apart from their chemical nature, mechanical properties of substrates strongly affect processes such as cell-matrix interaction, cell signaling and mechanotransduction [64,65]. Therefore, the viscoelastic properties of synthetic ECMs for cell culture must be carefully adjusted to promote cell growth.

Pure CNC hydrogels seem to be the most promising substrate for cell culture. Notably, the viscoelastic properties of the hybrids are rather similar since their G' values differ for no more than a factor of three (for the 50 mM MgCl_2 conc.) and yet they show rather different cell growth rates. Literature data for such soft substrates demonstrate that cell viability is not affected by the actual value of their elastic moduli [66–68] thus, given their similar viscoelastic properties, differences in cell spreading seem to be associated mainly with the microarchitecture of the gel network. Indeed, all three individual components (CNC, PEG and alginate) are known to be viable substrates for cell growth. Thus, while CNCs and NPs have a similar stiffness, they differ for a fundamental functional group (the amino group), and they show similar growth rates; on the other hand, NAs and CNCs have very similar chemical compositions but different microarchitectures and this is reflected on the largely different growth rates.

Conclusions

In this work, we demonstrate two results:

1. we showed that both the composite hydrogels made of CNC/linear amino-PEG and CNC/alginate are good substrates for the growth of a model cell line. However CNC/amino-PEG induces a much faster cell proliferation, despite the similar physical macroscopic properties of the two tested materials. This result suggests that the cells respond also to dynamic environmental cues not detectable by conventional techniques.
2. we introduced a novel DLS analysis implemented on commercial, single angle apparatus that is able to discriminate between gels having similar macroscopic mechanical properties but differing for their chemical composition and microscopic structural dynamics. As representative tests we investigated the dynamics of CNC-PEG and CNC-alginate materials. To prove the relationship between the dynamic DLS data and the microscopic hydrogel structure we exploited the peculiar characteristic of alginates to jellyify in the presence of Ca^{2+} but not with Mg^{2+} [43] since the smaller Mg^{2+} , at difference from Ca^{2+} , does not fit into the G boxes and establishes with alginate chains a weaker affinity-driven interaction ruled basically by Manning's theory [69]. By defining a phenomenological Figure of Merit (FOM), based on the short-time values of the 2nd order correlation function, we showed that its statistical properties contains information about the sol-gel transition and the material composition. We observed that the nanoscale dynamical properties are in some way retained when both the hydrogels attain stable and similar macroscopic properties. We suppose that the differences in their internal dynamics causally affect the hydrogel interaction with cells in culture. In fact, while CNC-PEG composites form a stable gel structure in a relatively short time and it induces a faster cell proliferation, the slowly equilibrating CNC-alginate hydrogels shows a longer induction time. Notably, cell proliferation depends on the stability of cell adhesion to the support and our results indicate that this stability is affected by the nanoscale phenomena. Cell adhesion and proliferation is a fundamental issue for the design of innovative hydrogels for human use (i.e. dispositive for tissue regeneration wound healing, drug delivery and organoids) and at present, the nanoscale behavior is often neglected. Conversely, this behavior seems to play an important role and here we provided a simple approach for its monitoring. Our method is characterized by a significantly better temporal (10's μs) and spatial (10's μm) resolution than the current state-of-the-art techniques commonly used for such analyses, such as rheometry, SAXS/SANS, and NMR, moreover it is directly implemented on simple DLS equipment without any modification. While phenomenological in nature, our approach is the

only one reported able to fully exploit the spatial and temporal resolution provided by DLS. It provides quantitative information about differences between materials that vary in specific parameters, like component ratios. Despite DLS is a well known technique, this is the first report where the statistical properties of the initial values of $g^{(2)}(t)$ is used to derive information about the chemical composition and the dynamical state of a material. Our proof-of-principle demonstration will pave the way for a much broader use of our approach. Dedicated models and computational tools are needed to fully understand the method's possibilities and limitations and will be developed in the future.

Supplementary Materials: The following supporting information can be downloaded at the website of this paper posted on [Preprints.org](https://www.preprints.org).

Author Contributions: A. Bartolomei: investigation, formal analysis, software, writing, review and editing, E. D'Amato: conceptualization, investigation, validation, writing, review and editing, M. Scarpa: Investigation, Funding Acquisition, Supervision, writing, review and editing, G. Bergamaschi: investigation, data curation, validation, writing, review and editing, A. Gori: investigation, data curation, validation, writing, review and editing, P. Bettotti: conceptualization, investigation, supervision, writing original draft. All authors have read and agreed to the published version of the manuscript.

Funding: This research was partially funded by the European Union - Next-GenerationEU - National Recovery and Resilience Plan (NRRP) – MISSION 4 COMPONENT 2, INVESTIMENT N. 1 – Green cellulose-based fire safe and lightweight Insulating materials (GAIA), Prot. n. P2022YKTR5, CUP N.E53D23017870001. We acknowledge financial support the Italian Ministry of Research (MUR), Project Title: Green Membranes from Nano-Cellulose-based materials for carbon dioxide sequestration (Menace@CO2), funded by Unione Europea, Next Generation EU, Mission 4 Component 2 - CUP E53D23005130006. Views and opinions expressed are however those of the author(s) only and do not necessarily reflect those of the European Union or European Commission. Neither the European Union nor the granting authority can be held responsible for them.

Data Availability Statement: DLS and rheometries raw data used in this article are available at https://drive.google.com/file/d/1-OyLK4-ADz1NnPX9Op_dAlTNcx15Ifkw/view?usp=sharing, <https://drive.google.com/file/d/1OItGV0ETq4vu82Uk8fkViyL1MEV0BI2U/view?usp=sharing>.

Acknowledgments: The authors acknowledge A. Foradori for the support in installing the CONTIN algorithm, A. Malcov, S. Y. Heydari and A. Rossi for the support in cell culture experiments.

Conflicts of Interest: The authors declare no conflicts of interest.

References

1. Ahmed, E.M. Hydrogel: Preparation, characterization, and applications: A review. *Journal of Advanced Research* **2015**, *6*, 105–121. <https://doi.org/10.1016/j.jare.2013.07.006>.
2. Madduma-Bandarage, U.S.K.; Madihally, S.V. Synthetic hydrogels: Synthesis, novel trends, and applications. *Journal of Applied Polymer Science* **2021**, *138*, 50376, [<https://onlinelibrary.wiley.com/doi/pdf/10.1002/app.50376>]. <https://doi.org/10.1002/app.50376>.
3. Zhang, Y.S.; Khademhosseini, A. Advances in engineering hydrogels. *Science* **2017**, *356*, eaaf3627. <https://doi.org/10.1126/science.aaf3627>.
4. Ullah, F.; Othman, M.B.H.; Javed, F.; Ahmad, Z.; Akil, H.M. Classification, processing and application of hydrogels: A review. *Materials Science and Engineering: C* **2015**, *57*, 414–433. <https://doi.org/10.1016/j.msec.2015.07.053>.
5. Hu, L.; Chee, P.L.; Sugiarto, S.; Yu, Y.; Shi, C.; Yan, R.; Yao, Z.; Shi, X.; Zhi, J.; Kai, D.; et al. Hydrogel-Based Flexible Electronics. *Advanced Materials* **2023**, *35*, 2205326, [<https://advanced.onlinelibrary.wiley.com/doi/pdf/10.1002/adma.202205326>]. <https://doi.org/10.1002/adma.202205326>.
6. Mikhailidi, A.; Ungureanu, E.; Tofanica, B.M.; Ungureanu, O.C.; Fortună, M.E.; Belosinschi, D.; Volf, I. Agriculture 4.0: Polymer Hydrogels as Delivery Agents of Active Ingredients. *Gels* **2024**, *10*. <https://doi.org/10.3390/gels10060368>.

7. Caló, E.; Khutoryanskiy, V.V. Biomedical applications of hydrogels: A review of patents and commercial products. *European Polymer Journal* **2015**, *65*, 252–267. 50 Years of European Polymer Journal, <https://doi.org/10.1016/j.eurpolymj.2014.11.024>.
8. Li, S.; Dong, S.; Xu, W.; Tu, S.; Yan, L.; Zhao, C.; Ding, J.; Chen, X. Antibacterial Hydrogels. *Advanced Science* **2018**, *5*, 1700527. <https://doi.org/10.1002/advs.201700527>.
9. Ghobril, C.; Grinstaff, M.W. The chemistry and engineering of polymeric hydrogel adhesives for wound closure: a tutorial. *Chem. Soc. Rev.* **2015**, *44*, 1820–1835. <https://doi.org/10.1039/C4CS00332B>.
10. Zhu, Y.; Romain, C.; Williams, C.K. Sustainable polymers from renewable resources. *Nature* **2016**, *540*, 354–362. <https://doi.org/10.1038/nature21001>.
11. Liu, J.; Cheng, F.; Grénman, H.; Spoljaric, S.; Seppälä, J.; E. Eriksson, J.; Willför, S.; Xu, C. Development of nanocellulose scaffolds with tunable structures to support 3D cell culture. *Carbohydrate Polymers* **2016**, *148*, 259–271. <https://doi.org/10.1016/j.carbpol.2016.04.064>.
12. Ferreira, F.V.; Otoni, C.G.; De France, K.J.; Barud, H.S.; Lona, L.M.; Cranston, E.D.; Rojas, O.J. Porous nanocellulose gels and foams: Breakthrough status in the development of scaffolds for tissue engineering. *Materials Today* **2020**, *37*, 126–141. <https://doi.org/10.1016/j.mattod.2020.03.003>.
13. Subhedar, A.; Bhadauria, S.; Ahankari, S.; Kargarzadeh, H. Nanocellulose in biomedical and biosensing applications: A review. *International Journal of Biological Macromolecules* **2021**, *166*, 587–600. <https://doi.org/10.1016/j.ijbiomac.2020.10.217>.
14. Maestri, C.A.; Abrami, M.; Hazan, S.; Chistè, E.; Golan, Y.; Rohrer, J.; Bernkop-Schnürch, A.; Grassi, M.; Scarpa, M.; Bettotti, P. Role of sonication pre-treatment and cation valence in the sol-gel transition of nano-cellulose suspensions. *Scientific Reports* **2017**, *7*, 11129. <https://doi.org/10.1038/s41598-017-11649-4>.
15. Maestri, C.A.; Bettotti, P.; Scarpa, M. Fabrication of complex-shaped hydrogels by diffusion controlled gelation of nanocellulose crystallites. *J. Mater. Chem. B* **2017**, *5*, 8096–8104. <https://doi.org/10.1039/C7TB01899A>.
16. Du, X.; Zhou, J.; Shi, J.; Xu, B. Supramolecular Hydrogelators and Hydrogels: From Soft Matter to Molecular Biomaterials. *Chemical Reviews* **2015**, *115*, 13165–13307. <https://doi.org/10.1021/acs.chemrev.5b00299>.
17. Bettotti, P.; Scarpa, M. Nanocellulose and Its Interface: On the Road to the Design of Emerging Materials. *Advanced Materials Interfaces* **2022**, *9*, 2101593. <https://doi.org/10.1002/admi.202101593>.
18. De France, K.J.; Hoare, T.; Cranston, E.D. Review of Hydrogels and Aerogels Containing Nanocellulose. *Chemistry of Materials* **2017**, *29*, 4609–4631. <https://doi.org/10.1021/acs.chemmater.7b00531>.
19. Curvello, R.; Raghuwanshi, V.S.; Garnier, G. Engineering nanocellulose hydrogels for biomedical applications. *Advances in Colloid and Interface Science* **2019**, *267*, 47–61. <https://doi.org/10.1016/j.cis.2019.03.002>.
20. Nascimento, D.M.; Nunes, Y.L.; Figueirêdo, M.C.B.; de Azeredo, H.M.C.; Aouada, F.A.; Feitosa, J.P.A.; Rosa, M.F.; Dufresne, A. Nanocellulose nanocomposite hydrogels: technological and environmental issues. *Green Chem.* **2018**, *20*, 2428–2448. <https://doi.org/10.1039/C8GC00205C>.
21. Du, H.; Liu, W.; Zhang, M.; Si, C.; Zhang, X.; Li, B. Cellulose nanocrystals and cellulose nanofibrils based hydrogels for biomedical applications. *Carbohydrate Polymers* **2019**, *209*, 130–144. <https://doi.org/10.1016/j.carbpol.2019.01.020>.
22. Hu, S.; Zhi, Y.; Shan, S.; Ni, Y. Research progress of smart response composite hydrogels based on nanocellulose. *Carbohydrate Polymers* **2022**, *275*, 118741. <https://doi.org/10.1016/j.carbpol.2021.118741>.
23. Deng, Y.; Xi, J.; Meng, L.; Lou, Y.; Seidi, F.; Wu, W.; Xiao, H. Stimuli-Responsive nanocellulose Hydrogels: An overview. *European Polymer Journal* **2022**, *180*, 111591. <https://doi.org/10.1016/j.eurpolymj.2022.111591>.
24. Strnad, S.; Zemljič, L. Cellulose–Chitosan Functional Biocomposites. *Polymers* **2023**, *15*, 425. <https://doi.org/10.3390/polym15020425>.
25. Wang, C.; Bai, J.; Tian, P.; Xie, R.; Duan, Z.; Lv, Q.; Tao, Y. The Application Status of Nanoscale Cellulose-Based Hydrogels in Tissue Engineering and Regenerative Biomedicine. *Front. Bioeng. Biotechnol.* **2021**, *9*, 732513. <https://doi.org/10.3389/fbioe.2021.732513>.
26. Heidarian, P.; Kaynak, A.; Paulino, M.; Zolfagharian, A.; Varley, R.J.; Kouzani, A.Z. Dynamic nanocellulose hydrogels: Recent advancements and future outlook. *Carbohydrate Polymers* **2021**, *270*, 118357. <https://doi.org/10.1016/j.carbpol.2021.118357>.
27. Liu, S.; Qamar, S.A.; Qamar, M.; Basharat, K.; Bilal, M. Engineered nanocellulose-based hydrogels for smart drug delivery applications. *International Journal of Biological Macromolecules* **2021**, *181*, 275–290. <https://doi.org/10.1016/j.ijbiomac.2021.03.147>.
28. Dong, S.; Roman, M. Fluorescently Labeled Cellulose Nanocrystals for Bioimaging Applications. *Journal of the American Chemical Society* **2007**, *129*, 13810–13811. <https://doi.org/10.1021/ja076196l>.

29. Jin, L.; Li, W.; Xu, Q.; Sun, Q. Amino-functionalized nanocrystalline cellulose as an adsorbent for anionic dyes. *Cellulose* **2015**, *22*, 2443–2456. <https://doi.org/10.1007/s10570-015-0649-4>.
30. Palaganas, N.B.; Mangadlao, J.D.; de Leon, A.C.C.; Palaganas, J.O.; Pangilinan, K.D.; Lee, Y.J.; Advincula, R.C. 3D Printing of Photocurable Cellulose Nanocrystal Composite for Fabrication of Complex Architectures via Stereolithography. *ACS Applied Materials & Interfaces* **2017**, *9*, 34314–34324. <https://doi.org/10.1021/acsami.7b09223>.
31. Kalossaka, L.M.; Mohammed, A.A.; Sena, G.; Barter, L.; Myant, C. 3D printing nanocomposite hydrogels with lattice vascular networks using stereolithography. *Journal of Materials Research* **2021**, *36*, 4249–4261. <https://doi.org/10.1557/s43578-021-00411-2>.
32. Bai, C.; Tang, A.; Zhao, S.; Liu, W. Flexible nanocellulose/poly(ethylene glycol) diacrylate hydrogels with tunable Poisson's ratios by masking and photocuring. *BioResources* **2020**, *15*, 3307–3319. <https://doi.org/10.15376/biores.15.2.3307-3319>.
33. Tang, A.; Ji, J.; Li, J.; Liu, W.; Wang, J.; Sun, Q.; Li, Q. Nanocellulose/PEGDA Aerogels with Tunable Poisson's Ratio Fabricated by Stereolithography for Mouse Bone Marrow Mesenchymal Stem Cell Culture. *Nanomaterials* **2021**, *11*, 603. <https://doi.org/10.3390/nano11030603>.
34. Monfared, M.; Mawad, D.; Rnjak-Kovacina, J.; Stenzel, M.H. 3D bioprinting of dual-crosslinked nanocellulose hydrogels for tissue engineering applications. *J. Mater. Chem. B* **2021**, *9*, 6163–6175. <https://doi.org/10.1039/D1TB00624J>.
35. Iman, M.; Barati, A.; Safari, S. Characterization, in vitro antibacterial activity, and toxicity for rat of tetracycline in a nanocomposite hydrogel based on PEG and cellulose. *Cellulose* **2020**, *27*, 347–356. <https://doi.org/10.1007/s10570-019-02783-5>.
36. Yin, A.; Yang, J. Cross-Linking Dynamics of Cellulose Nanofibrils-Based Transient Network Hydrogels: A Study of pH Dependence. *Macromolecular Chemistry and Physics* **2017**, *218*, 1600584. <https://doi.org/10.1002/macp.201600584>.
37. Yang, J.; Zhang, X.; Ma, M.; Xu, F. Modulation of Assembly and Dynamics in Colloidal Hydrogels via Ionic Bridge from Cellulose Nanofibrils and Poly(ethylene glycol). *ACS Macro Letters* **2015**, *4*, 829–833. <https://doi.org/10.1021/acsmacrolett.5b00422>.
38. Monfared, M.; Mawad, D.; Rnjak-Kovacina, J.; Stenzel, M.H. 3D bioprinting of dual-crosslinked nanocellulose hydrogels for tissue engineering applications. *Journal of Materials Chemistry B* **2021**, *9*, 6163 – 6175. Cited by: 35, <https://doi.org/10.1039/d1tb00624j>.
39. Tehrani, Z.; Nordli, H.R.; Pukstad, B.; Gethin, D.T.; Chinga-Carrasco, G. Translucent and ductile nanocellulose-PEG bionanocomposites—A novel substrate with potential to be functionalized by printing for wound dressing applications. *Industrial Crops and Products* **2016**, *93*, 193 – 202. Cited by: 42, <https://doi.org/10.1016/j.indcrop.2016.02.024>.
40. Silva, R.d.; Sierakowski, M.R.; Bassani, H.P.; Zawadzki, S.F.; Pirich, C.L.; Ono, L.; de Freitas, R.A. Hydrophilicity improvement of mercerized bacterial cellulose films by polyethylene glycol graft. *International Journal of Biological Macromolecules* **2016**, *86*, 599 – 605. Cited by: 31, <https://doi.org/10.1016/j.ijbiomac.2016.01.115>.
41. Donati, I.; Christensen, B.E. Alginate-metal cation interactions: Macromolecular approach. *Carbohydrate Polymers* **2023**, *321*, 121280. <https://doi.org/10.1016/j.carbpol.2023.121280>.
42. Donati, I.; Asaron, F.; Paoletti, S. Experimental evidence of counterion affinity in alginates: The case of nongelling ion Mg²⁺. *Journal of Physical Chemistry B* **2009**, *113*, 12877 – 12886. <https://doi.org/10.1021/jp902912m>.
43. Tordi, P.; Ridi, F.; Samori, P.; Bonini, M. Cation-Alginate Complexes and Their Hydrogels: A Powerful Toolkit for the Development of Next-Generation Sustainable Functional Materials. *Advanced Functional Materials*, *n/a*, 2416390, [<https://advanced.onlinelibrary.wiley.com/doi/pdf/10.1002/adfm.202416390>]. <https://doi.org/10.1002/adfm.202416390>.
44. Raghuwanshi, V.S.; Garnier, G. Characterisation of hydrogels: Linking the nano to the microscale. *Advances in Colloid and Interface Science* **2019**, *274*, 102044. <https://doi.org/10.1016/j.cis.2019.102044>.
45. Mendoza, L.; Batchelor, W.; Tabor, R.F.; Garnier, G. Gelation mechanism of cellulose nanofibre gels: A colloids and interfacial perspective. *Journal of Colloid and Interface Science* **2018**, *509*, 39–46. <https://doi.org/10.1016/j.jcis.2017.08.101>.
46. Armstrong, M.J.; Beris, A.N.; Rogers, S.A.; Wagner, N.J. Dynamic shear rheology of a thixotropic suspension: Comparison of an improved structure-based model with large amplitude oscillatory shear experiments. *Journal of Rheology* **2016**, *60*, 433–450, [https://pubs.aip.org/sor/jor/article-pdf/60/3/433/16747170/433_1_online.pdf]. <https://doi.org/10.1122/1.4943986>.

47. Jakeman, E. Photon Correlation. In *Photon Correlation and Light Beating Spectroscopy*; Cummins, H.Z.; Pike, E.R., Eds.; Springer Science + Business Media, LLC: New York, 1974.
48. Pusey, P.; Van Megen, W. Dynamic light scattering by non-ergodic media. *Physica A: Statistical Mechanics and its Applications* **1989**, *157*, 705–741. [https://doi.org/10.1016/0378-4371\(89\)90063-0](https://doi.org/10.1016/0378-4371(89)90063-0).
49. Shibayama, M.; Norisuye, T. Gel formation analyses by dynamic light scattering. *Bulletin of the Chemical Society of Japan* **2002**, *75*, 641 – 659. Cited by: 144, <https://doi.org/10.1246/bcsj.75.641>.
50. Abou, B.; Bonn, D.; Meunier, J. Aging dynamics in a colloidal glass. *Phys. Rev. E* **2001**, *64*, 021510. <https://doi.org/10.1103/PhysRevE.64.021510>.
51. Scheffold, F.; Skipetrov, S.; Romer, S.; Schurtenberger, P. Diffusing-wave spectroscopy of nonergodic media. *Physical Review E - Statistical, Nonlinear, and Soft Matter Physics* **2001**, *63*, 061404/1 – 061404/11. Cited by: 106; All Open Access, Green Open Access, <https://doi.org/10.1103/PhysRevE.63.061404>.
52. Urquidi, O.; Barbosa, N.; Brazard, J.; Adachi, T.B.M. Toward time resolved dynamic light scattering microscopy: Retrieving particle size distributions at high temporal resolutions. *Review of Scientific Instruments* **2023**, *94*, 083101, [https://pubs.aip.org/aip/rsi/article-pdf/doi/10.1063/5.0160156/18067345/083101_1_5.0160156.pdf]. <https://doi.org/10.1063/5.0160156>.
53. Fahimi, Z.; Aangenendt, F.J.; Voudouris, P.; Mattsson, J.; Wyss, H.M. Diffusing-wave spectroscopy in a standard dynamic light scattering setup. *Physical Review E* **2017**, *96*, 062611. <https://doi.org/10.1103/PhysRevE.96.062611>.
54. Badruddoza, A.Z.M.; MacWilliams, S.V.; Sebben, D.A.; Krasowska, M.; Beattie, D.; Durian, D.J.; Ferri, J.K. Diffusing wave spectroscopy (DWS) methods applied to double emulsions. *Current Opinion in Colloid & Interface Science* **2018**, *37*, 74–87. Surface analysis techniques, <https://doi.org/10.1016/j.cocis.2018.06.006>.
55. Hassan, P.A.; Rana, S.; Verma, G. Making Sense of Brownian Motion: Colloid Characterization by Dynamic Light Scattering. *Langmuir* **2015**, *31*, 3–12. <https://doi.org/10.1016/j.cocis.2018.06.006>.
56. Höhler, R.; Cohen-Addad, S.; Durian, D.J. Multiple light scattering as a probe of foams and emulsions. *Current Opinion in Colloid & Interface Science* **2014**, *19*, 242–252. <https://doi.org/10.1016/j.cocis.2014.04.005>.
57. Isogai, A.; Saito, T.; Fukuzumi, H. TEMPO-oxidized cellulose nanofibers. *Nanoscale* **2011**, *3*, 71–85. <https://doi.org/10.1039/C0NR00583E>.
58. Capes-Davis, A.; Freshney, R., Eds. *Freshney's Culture of Animal Cells*, 8 ed.; Wiley-Blackwell, 2021.
59. Truong, C.; Oudre, L.; Vayatis, N. Selective review of offline change point detection methods. *Signal Processing* **2020**, *167*, 107299. <https://doi.org/10.1016/j.sigpro.2019.107299>.
60. Hong, T.; Yin, J.Y.; Nie, S.P.; Xie, M.Y. Applications of infrared spectroscopy in polysaccharide structural analysis: Progress, challenge and perspective. *Food Chemistry: X* **2021**, *12*, 100168. <https://doi.org/10.1016/j.fochx.2021.100168>.
61. Kotov, N.; Larsson, P.A.; Jain, K.; Abitbol, T.; Cernescu, A.; Wågberg, L.; Johnson, C.M. Elucidating the fine-scale structural morphology of nanocellulose by nano infrared spectroscopy. *Carbohydrate Polymers* **2023**, *302*, 120320. <https://doi.org/10.1016/j.carbpol.2022.120320>.
62. Li, M.C.; Wu, Q.; Song, K.; Qing, Y.; Wu, Y. Cellulose Nanoparticles as Modifiers for Rheology and Fluid Loss in Bentonite Water-based Fluids. *ACS Applied Materials & Interfaces* **2015**, *7*, 5006–5016. <https://doi.org/10.1021/acsami.5b00498>.
63. Abitbol, T.; Mijlkovic, A.; Malafronte, L.; Stevanic, J.S.; Larsson, P.T.; Lopez-Sanchez, P. Cellulose nanocrystal/low methoxyl pectin gels produced by internal ionotropic gelation. *Carbohydrate Polymers* **2021**, *260*, 117345. <https://doi.org/10.1016/j.carbpol.2020.117345>.
64. Elosegui-Artola, A. The extracellular matrix viscoelasticity as a regulator of cell and tissue dynamics. *Current Opinion in Cell Biology* **2021**, *72*, 10–18. Cell Dynamics, <https://doi.org/10.1016/j.ceb.2021.04.002>.
65. Caliri, S.R.; Burdick, J.A. A practical guide to hydrogels for cell culture. *Nature Methods* **2016**, *13*, 405–414. <https://doi.org/10.1038/nmeth.3839>.
66. Zhang, C.; Tan, Y.; Feng, J.; Huang, C.; Liu, B.; Fan, Z.; Xu, B.; Lu, T. Exploration of the Effects of Substrate Stiffness on Biological Responses of Neural Cells and Their Mechanisms. *ACS Omega* **2020**, *5*, 31115–31125. <https://doi.org/10.1021/acsomega.0c04279>.
67. Fan, Y.; Sun, Q.; Li, X.; Feng, J.; Ao, Z.; Li, X.; Wang, J. Substrate Stiffness Modulates the Growth, Phenotype, and Chemoresistance of Ovarian Cancer Cells. *Front. Cell Dev. Biol.* **2021**, *9*, 7118834. <https://doi.org/10.3389/fcell.2021.718834>.

68. Guo, A.; Wang, B.; Lyu, C.; Li, W.; Wu, Y.; Zhu, L.; Bi, R.; Huang, C.; Li, J.J.; Du, Y. Consistent apparent Young's modulus of human embryonic stem cells and derived cell types stabilized by substrate stiffness regulation promotes lineage specificity maintenance. *Cell Regeneration* **2020**, *9*. <https://doi.org/10.1186/s13619-020-00054-4>.
69. Borgogna, M.; Skjåk-Bræk, G.; Paoletti, S.; Donati, I. On the Initial Binding of Alginate by Calcium Ions. The Tilted Egg-Box Hypothesis. *The Journal of Physical Chemistry B* **2013**, *117*, 7277–7282. PMID: 23713959, <https://doi.org/10.1021/jp4030766>.

Disclaimer/Publisher's Note: The statements, opinions and data contained in all publications are solely those of the individual author(s) and contributor(s) and not of MDPI and/or the editor(s). MDPI and/or the editor(s) disclaim responsibility for any injury to people or property resulting from any ideas, methods, instructions or products referred to in the content.